Impacts of bottom corrugations on a dense Antarctic outflow: NW Ross Sea

R. D. Muench,[1] A. K. Wåhlin,[2] T. M. Özgökmen,[3] R. Hallberg,[4] and L. Padman[5]

Received 13 October 2009; accepted 5 November 2009; published 9 December 2009.

[1] Prominent seabed corrugations, axially oriented roughly down-slope, are present along the Antarctic continental slope. We use analytical and numerical model results to assess the potential impact of these corrugations on outflows of dense shelf water that contribute to Antarctic Bottom Water. Down-slope flow increases with increasing corrugation height and varies with along-slope wavelength. For parameters appropriate to the northwest Ross Sea, where heights and wavelengths are ∼10–20 m and ∼1.5 km, respectively, we estimate that the corrugations increase the down-slope transport of dense water, relative to the smooth bottom case, by ∼13%. Corrugations enhance entrainment and reduce along-slope speed of the dense outflow. Larger amplitude corrugations (∼100 m) observed in other regions may impact outflows elsewhere around the poorly mapped Antarctic continental margin. Our results emphasize the need to consider small-scale local topography when modeling dense outflows. **Citation:** Muench, R. D., A. K. Wåhlin, T. M. Özgökmen, R. Hallberg, and L. Padman (2009), Impacts of bottom corrugations on a dense Antarctic outflow: NW Ross Sea, *Geophys. Res. Lett.*, *36*, L23607, doi:10.1029/2009GL041347.

1. Introduction

[2] High resolution bathymetric surveys around Antarctica frequently identify "corrugations" over the continental shelf and upper slope that are axially oriented roughly down-slope [*Davey and Jacobs*, 2007; *Noormets et al.*, 2009]. These features have typical trough-to-crest heights H_C of 10–100 m and along-slope trough-to-trough wavelengths λ_C of order 1 km (Figure 1).

[3] Dense shelf water, formed through surface cooling and brine rejection from sea ice growth and through sub-ice-shelf processes, exits over the shelf break and slope as dense outflows. These outflows contribute to the production of Antarctic Bottom Water (AABW), the dominant abyssal water mass in the world ocean [*Johnson*, 2008]. Here we explore the hypothesis, suggested by recent model results [*Wåhlin*, 2002, 2004a; *Özgökmen and Fischer*, 2008], that corrugations on the slope can enhance the down-slope transport of dense water. Our study is motivated by bathymetric and oceanographic data from the Antarctic Slope ("AnSlope") experiment in the northwest Ross Sea [*Gordon et al.*, 2004, 2009], but bears on dense outflows elsewhere around Antarctica including the Weddell Sea [*Gordon*, 1998; *Foldvik et al.*, 2004] and the Adèlie Land Coast [*Rintoul*, 1998].

2. NW Ross Sea Dense Outflow

[4] Dense high salinity shelf water (HSSW) formed on the continental shelf of the western Ross Sea flows northwards to the shelf break along several troughs. The HSSW feeds dense, bottom-trapped outflows that can be traced flowing westward along the continental slope [*Gordon et al.*, 2009]. We focus here on the westernmost outflow, from the Drygalski Trough (Figure 1), which was extensively documented by the AnSlope field program. The pathway and volume transport of this outflow were estimated for summer 2003 using potential temperature θ and salinity S as water mass tracers and detided currents derived from a lowered acoustic Doppler current profiler (LADCP) [*Gordon et al.*, 2004, 2009]. Outflow current speed was ∼0.5 m s^{-1} and the associated volume transport was ∼1.7 Sv, of which ∼0.4 Sv was HSSW. The outflow varied in thickness from ∼30 m near the shelf break during neap tides to more than 200 m farther down-slope during spring tides [*Muench et al.*, 2009]. This variability reflects entrainment and a pronounced fortnightly variability in locally strong tidal currents [*Muench et al.*, 2009].

[5] The NW Ross Sea area seafloor (Figure 1) was mapped using a vessel-mounted multibeam system [*Davey and Jacobs*, 2007]. Typical depth over the continental shelf is ∼500 m. The continental slope under the Drygalski Trough outflow is steep; ∼1:10 directly down-slope from its mouth, increasing to ∼1:6 within ∼10 km to the west. An extensive field of seafloor corrugations underlies the outflow over most of the slope (∼500–2000 m depths). The most obvious corrugations trend down-slope and have typical along-slope wavelengths λ_C of ∼1.5 km and vertical trough-to-crest heights H_C of ∼10–20 m (Figure 1). Examination of their origins exceeds the scope of this paper. However, we speculate, in agreement with *Davey and Jacobs* [2007], that they may reflect current scour associated with jet-like down-slope flow events of dense water as reported by *Gordon et al.* [2004].

3. Analytical Model

[6] We consider the model geometry shown in Figure 2, following *Wåhlin* [2004a]. Figure 2 and the following discussion are for the southern hemisphere case. The down-slope and westward along-slope directions are x and y, respectively. The seafloor has a constant slope s_b downward in the x-direction, parallel to the corrugation axes. The corrugations consist of troughs and ridges extending from

[1]Earth and Space Research, Seattle, Washington, USA.
[2]Department of Earth Sciences, University of Gothenburg, Gothenburg, Sweden.
[3]RSMAS, University of Miami, Miami, Florida, USA.
[4]Geophysical Fluid Dynamics Laboratory, NOAA, Princeton, New Jersey, USA.
[5]Earth and Space Research, Corvallis, Oregon, USA.

0094-8276/09/2009GL041347$05.00

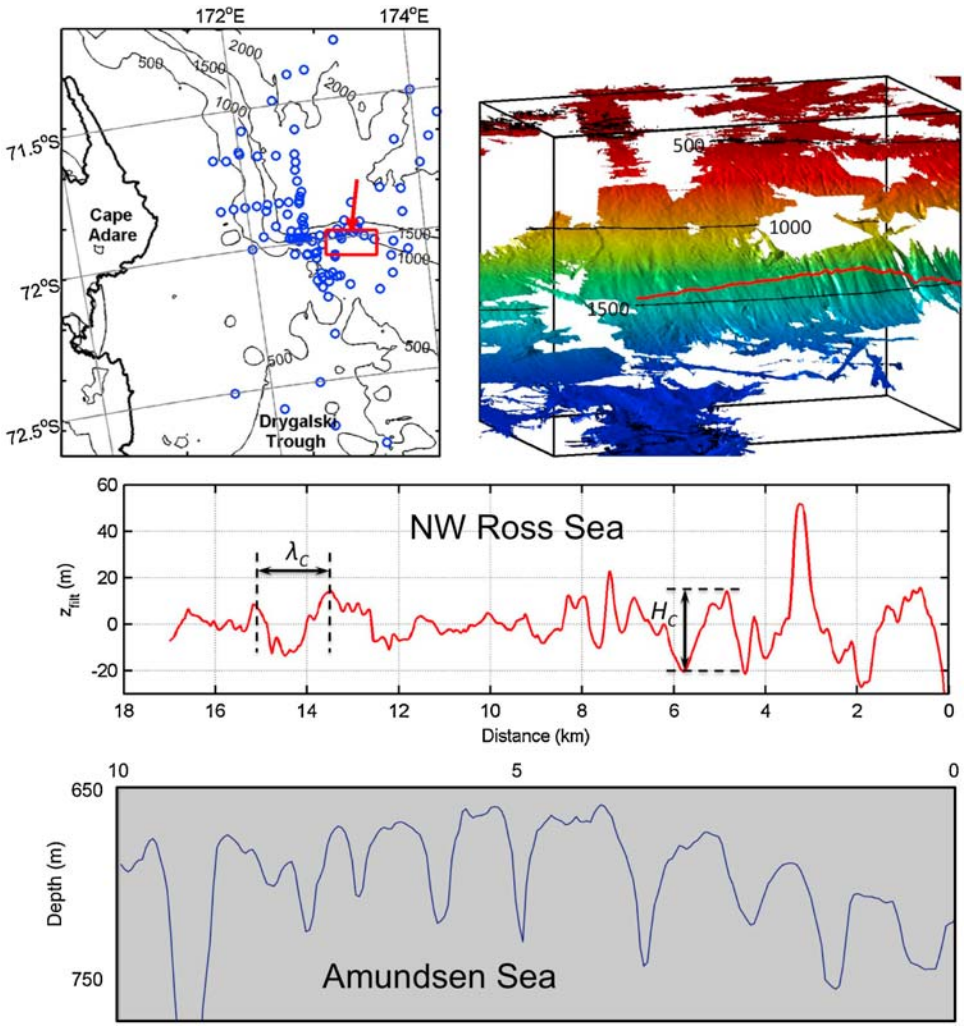

Figure 1. (top left) Bathymetry in the northwest Ross Sea. Red box shows region of high resolution multibeam bathymetry data [*Davey and Jacobs*, 2007] shown in other plots. Blue circles show locations of CTD/LADCP profiles used to define the path of the dense water outflow from the Drygalski Trough sill northwestward along the continental slope. (top right) 3-D multibeam bathymetry for the region shown on the map, viewed from the NNE (red arrow on map): red shading indicates upper slope and shelf; dark blue is deep water. Black lines show 500, 1000 and 1500 isobaths. Red line near 1500 m shows location of depth transect across the corrugations. (middle) High-pass filtered bathymetry along the transect shown in Figure 1 (top right), with definitions of λ_C and H_C. (bottom) Along-slope bathymetric trace from the Amundsen Sea upper slope [*Noormets et al.*, 2009].

the shelf break to the deep sea, with along-slope wavelength λ_C and amplitude $H_C/2$ (Figure 1). Bottom elevation is $h_C(x, y) = s_b x + \frac{H_C}{2} \cos(2\pi \frac{y}{\lambda_C})$, dense layer thickness is $h_0(y)$, and the interface η between the dense layer and ambient fluid approaches $\eta = h_C + h_0$ moving downslope.

[7] A dense outflow is viewed here as a stationary, geostrophic along-slope bottom flow with a down-slope frictional component. In the presence of corrugations, down-slope transport converges in each trough, a portion then flowing down-slope within the trough rather than continuing along isobaths. The tendency for flow to parallel isobaths and exit the troughs [*Nof*, 1983; *Wåhlin*, 2004b] is balanced by bottom drag within the troughs that generates an Ekman transport to the right of the flow direction and counters the tendency to parallel isobaths. If down-slope speed is sufficiently large, the two cross-corrugation flows will balance each other [*Wåhlin*, 2002, 2004a]. In this case the main flow is down-slope along the trough, and secondary cross-corrugation flows are superimposed on this motion (Figure 2). The cross-corrugation flow component in the benthic boundary layer is the Ekman transport $m_E(y)$ to the right of the down-slope flow, in the negative y-direction. Cross-corrugation flow above the boundary layer is $vh_0(y)$, to the left of the down-slope flow (where v is cross-corrugation velocity in the y-direction). Steady down-slope flow can be maintained if $m_E + vh_0 = 0$, where $v = \frac{g' s_b}{f}$, $m_E = \delta_E u_G$, g' is reduced gravity for a dense outflow underlying less dense ambient water, f is the Coriolis parameter, and u_G the geostrophic speed in the down-slope (x) direction. Ekman benthic layer thickness δ_E can be estimated as $\delta_E = C_D \frac{g' s_b}{f^2}$ [*Wåhlin and Walin*, 2001; *Wåhlin*, 2004a]. Parameter values

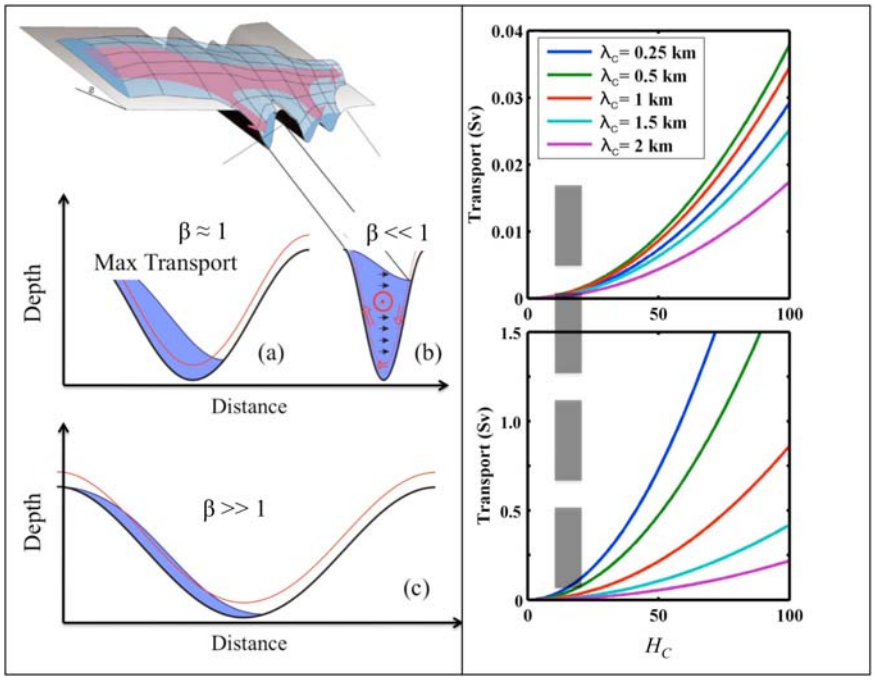

Figure 2. (left) Circulation computed in a corrugation trough using an analytical model (see text). The schematic shows model geometry. Red arrows indicate flow direction and blue shows dense water. Cases a, b and c show flow pattern at the mouth of the trough for $\beta \approx 1$ (maximum transport), $\beta \ll 1$ and $\beta \gg 1$, respectively. For case b the red circle indicates down-trough flow, open red arrows indicate Ekman transport induced by the downslope flow, and black arrows show the return flow. The blue field shows dense water, the fine red line shows Ekman layer thickness, and the thick black line shows the seafloor. (right) Downslope transport as a function of corrugation wavelength λ_C in km and height H_C in m (top) for a single corrugation and (bottom) for a 25 km long corrugated slope. Broad dashed line indicates approximate H_C for the NW Ross Sea. Values were computed using δ_E and s_b appropriate for the Ross Sea (see text).

typical for the Ross Sea ($C_D = 2.5 \times 10^{-3}$, $g' = 2 \times 10^{-3}$ m s^{-2}, $s_b = 0.1$ and $f = 1.3 \times 10^{-4}$ s^{-1} [see *Muench et al.*, 2009]) yield δ_E = 30 m. The balance can also be expressed as [*Wåhlin*, 2002, 2004a]

$$-\delta_E \frac{g'}{f} \frac{\partial}{\partial y}(h_C + h_0) + h_0(y) \frac{g' s_b}{f} = 0, \quad (1)$$

where $u_G = \frac{g'}{f} \frac{\partial}{\partial y} (h_C + h_O)$. Equation (1) can be rewritten as $\frac{\partial h_0}{\partial y} - \beta \frac{h_0(y)}{\lambda_C} = \frac{\partial h_C}{\partial y}$, where

$$\beta = \frac{\lambda_C s_b}{\delta_E}. \quad (2)$$

Here, β is a geometrical non-dimensional number expressing the ratio between the cross-corrugation Ekman transport and return flow scales [*Wåhlin*, 2004a].

[8] Solutions to equation (1) reveal trough circulation regimes that vary with β (Figure 2a): $\beta \ll 1$, a comparatively slow but thick flow with a small cross-corrugation slope of the dense outflow interface; $\beta \approx 1$, a medium thickness flow having maximum down-slope transport in the corrugations; and, $\beta \gg 1$, a comparatively thin flow with a steeply sloping interface. Corrugation parameters typifying the NW Ross Sea (λ_C = 1.5 km, s_b = 0.1, δ_E = 30 m) yield β = 5, within the maximum transport range. Single-trough analytical solutions derived over ranges of λ_C and H_C that encompass likely cases, including the Ross Sea, illustrate the dependence of downslope transport on these parameters and indicate that $\lambda_C \sim$ 0.5 km yields optimal down-slope flow (Figure 2, right). Extension of these values to a 25-km long corrugated slope consistent with the Ross Sea case, and assuming that the benthic layer consists primarily of HSSW, yields a downslope HSSW transport of ~0.05 Sv, or ~13% of the ~0.4 Sv mean HSSW transport estimated by *Gordon et al.* [2009]. Transport down a 25-km long slope increases rapidly with increasing H_C, approaching ~0.25–0.5 Sv for H_C = 50 m. Corrugations having heights approaching 40 m were present toward the western end of the transect (Figure 1), however, these were not representative of the entire slope.

4. Numerical Simulations

[9] Two numerical models were used as a qualitative check on the analytical results and to better visualize flow behavior down a corrugated slope. The impact of varying λ_C on down-slope flow was addressed using the nek5000 model [*Fischer*, 1997], which has been previously employed for dense outflow simulations [*Özgökmen et al.*, 2004; *Özgökmen and Fischer*, 2008] and integrates the three-dimensional non-hydrostatic Boussinesq equations using the spectral element method. A second series of simulations investigated the impact of varying H_C on downslope flow using the Generalized Ocean Layer Dynamics (GOLD) model, an isopycnal-coordinate, hydrostatic model. Use of these two different models allows us to identify robust (model-independent) features of the solutions and to better understand the limitations of different approaches. The

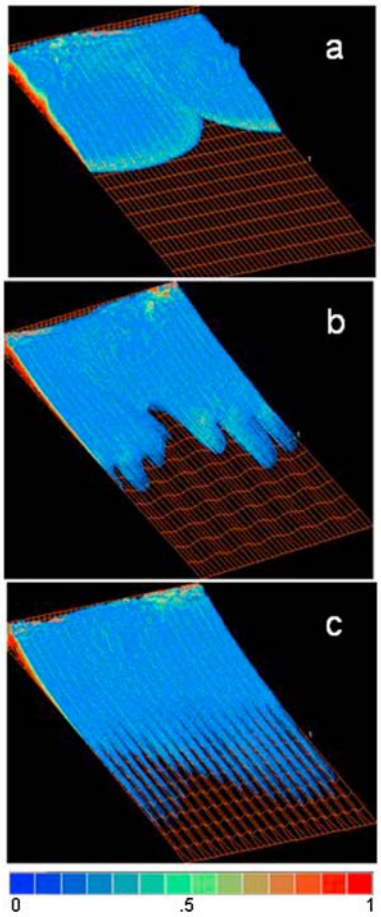

Figure 3. Three-dimensional view of the non-dimensional shelf water density perturbation from three nek5000 model simulations, each at the same time step, for: (a) smooth bottom, no corrugations, showing downslope Ekman drainage; (b) H_C = 200 m and λ_C = 2 km, showing enhancement of downslope flow; and (c) H_C = 200 m and λ_C = 700 m, showing still greater enhancement of downslope flow with decreasing λ_C. An animation of the complex evolution of the density perturbation field for case b is available from http://www.rsmas.miami.edu/personal/tamay/3D/corrugations-b.gif.

hydrostatic GOLD model reveals interactions between small-scale flows and larger scale features of the circulation (e.g., mesoscale irregularities, as noted in the text), and also can represent under-resolved dynamics of this nature in future OGCMs. In contrast, Nek5000 integrates Boussinesq equations and relies more on resolved than parameterized dynamics.

[10] The nek5000 model simulated a physical domain with dimensions of 12 km, 6 km and 2 km in the down-slope, along-slope and vertical directions, respectively, and assumed a 2 km deformation radius for the outflow. A ~400 m thick flow was introduced into the interior onto a bottom slope s_b = 0.1. The upper boundary condition was rigid lid and free slip. The model mesh consisted of 5,184 elements and 8th-order polynomials, yielding ~2.7×10^6 spatial points with the mesh spacing $\delta = (\Delta x\ \Delta y\ \Delta z)^{1/3}$ varying within the range 9.8 m $\leq \delta \leq$ 34 m. Five simulations were carried out, including a smooth bottom case and two cases with H_C ~200 m and varying λ_C (Figure 3). The outflow undergoes geostrophic adjustment until reaching a final state characterized by mesoscale fluctuations along the upper slope and a slow, downslope near-bottom Ekman flux. The corrugations markedly enhance down-slope flow relative to the smooth bottom case (Figure 3). This flow increased as λ_C was decreased from 2 km to 700 m, passing through the "realistic" 1.5 km value for the Ross Sea and approaching 0.5 km where the analytical model predicts optimal downslope transport. These results confirm an enhancement of downslope flow by corrugations and an increase in transport with decreasing λ_C, consistent with the analytical results.

[11] The GOLD model simulations were forced by a 0.15 Sv outflow of dense water introduced at the top of a slope with s_b = 0.1 (Figure 4). The outflow is 0.2 kg m^{-3} denser than ambient water, consistent with *Gordon et al.* [2009] and with values used in the above analytical calculations. Inflow was geostrophically balanced, similar to the "DOME" configuration [*Legg et al.*, 2006], and the 250 m horizontal resolution resolved the ~2 km outflow deformation radius. Shear-driven mixing was provided through the parameterization of *Jackson et al.* [2008]. Results from a subset of the simulations are illustrated in the horizontal plane

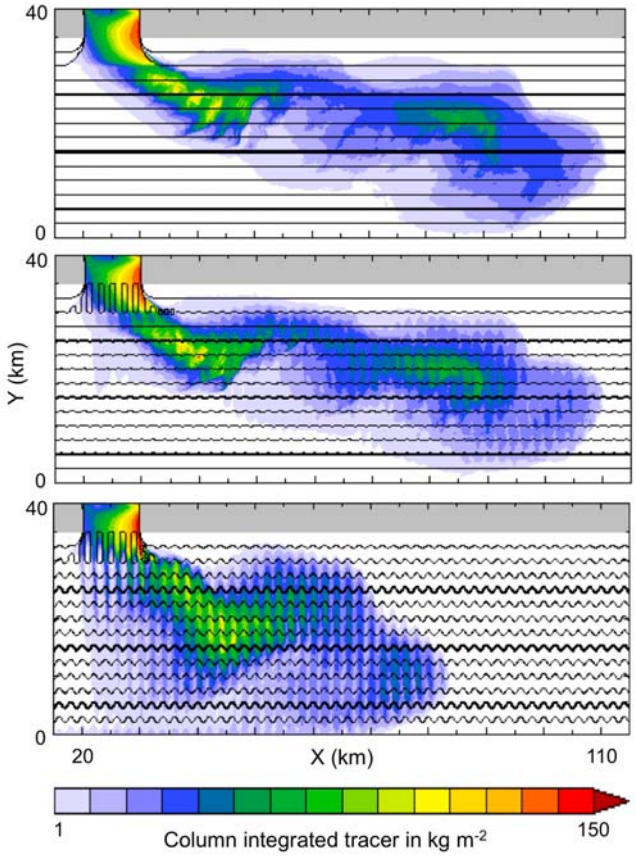

Figure 4. Horizontal distribution of column-integrated tracer density for a tracer with initial concentration of 1 kg m^{-3} introduced into the dense water outflow at the sill, using the GOLD model spun up for 4 days, for: (upper) smooth bottom case; (middle) case with λ_C = 2 km and H_C = 20 m; and (lower) case for λ_C = 2 km and h_C = 100 m. Impact of corrugations increases dramatically with increasing h_C.

using the column-integrated concentration of a tracer having an initial concentration in the dense outflow of 1 kg m^{-3} and zero in the ambient water (Figure 4). Isobaths on the figures emphasize the coincidence between the corrugations and downslope plumes. The smooth bottom results resemble those obtained using nek5000, with mesoscale instabilities on the upper slope. For H_C = 20 m, the effect on the outflow was evident but small. Increasing H_C to 100 m markedly enhanced downslope descent of the outflow and increased lateral spreading. This case resembles the H_C = 200 m, $\lambda_C \sim$700 m run with the nek5000 model (Figure 3c). Tracer concentrations within the plume drop over shorter distances as H_C is increased, reflecting enhanced entrainment of ambient (tracer-free) water. Increasing λ_C in the GOLD runs (not shown) decreased the impacts, consistent with the analytical and nek5000 model results (Figures 2 and 3).

5. Discussion and Conclusions

[12] Seabed corrugations enhance the down-slope flow component and correspondingly decrease along-slope transport associated with a dense, bottom-trapped outflow. Down-slope flow increases with increasing corrugation height H_C, and with decreasing wavelength λ_C down to an optimal value near ~0.5 km. These transport changes modify the location where dense overflow water is delivered to the deep ocean. Based on the tracer distributions in the GOLD model runs, corrugations enhance entrainment of ambient water into the outflow such that lower density outflow water is delivered to the bottom of the slope than for the smooth bottom case: this result is consistent with recent laboratory studies [*Davies et al.*, 2006; *Wåhlin et al.*, 2008; *Darelius*, 2008]. Enhanced down-slope flow due to corrugations might contribute to the anomalously large 35° down-slope flow angle reported for the NW Ross Sea dense outflow [*Gordon et al.*, 2009].

[13] The nek5000 and GOLD model runs (Figures 3 and 4) both show generation of mesoscale instabilities in the outflow, whether or not corrugations are present. Recent numerical studies of Antarctic dense outflows [e.g., *Padman et al.*, 2009] also show instabilities, and note the importance of flow variability due to "external" processes such as tides. These results suggest that the steady-state assumption of the analytical model (Figure 2) may not be appropriate to real dense outflows, and raise the possibility that the role of corrugations in setting mean outflow properties differs significantly from the idealized results reported here.

[14] Given the generally low quality of bathymetric mapping around most of the Antarctic continental margin, we cannot speculate on which density outflows might be influenced by corrugations. This study suggests, however, the length scales of features that are likely to impact outflows.

[15] Impacts described above might apply equally in the case of Ice Shelf Water (ISW) plumes that rise along the sloping bases of ice shelves after gaining buoyancy from addition of fresh water through basal melt [e.g., *Holland and Jenkins*, 1999]. Here, corrugations are associated with basal crevasses formed, for example, through tidal flexure at the ice shelf grounding line then migrating offshore with the mean ice shelf flow. While observations of crevasse dimensions are sparse, typical values for H_C and λ_C are ~10–100 m and ~1 km, respectively, suggesting that these may significantly impact buoyant plumes beneath the ice shelves.

[16] **Acknowledgments.** This study was supported by the NSF (grants OPP-01256023 and ANT-0440656 to ESR, and grant OCE 0611579 to RSMAS), ONR (grants N00014-03-1-0067 and N00014-08-1-0548 to ESR), NOAA, and the Swedish Research Council. This is Earth and Space Research contribution 140.

References

Darelius, E. (2008), Topographic steering of dense overflows: Laboratory experiments with V-shaped ridges and canyons, *Deep Sea Res., Part I*, *55*, 1021–1034, doi:10.1016/j.dsr.2008.04.008.

Davey, F. J., and S. S. Jacobs (2007), Influence of submarine morphology on bottom water flow across the western Ross Sea continental margin, Antarctica, in *A Keystone in a Changing World*, edited by A. K. Cooper and C. R. Raymond, *U.S. Geol. Surv. Open File Rep., 2007-1047*, doi:10.3133/of2007-1047.srp067.

Davies, P., A. Wåhlin, and Y. Guo (2006), Laboratory and analytical model studies of the Faroe Bank Channel deep-water outflow, *J. Phys. Oceanogr.*, *36*, 1348–1364, doi:10.1175/JPO2917.1.

Fischer, P. F. (1997), An overlapping Schwartz method for spectral element solution of the incompressible Navier-Stokes equations, *J. Comput. Phys.*, *133*, 84–101, doi:10.1006/jcph.1997.5651.

Foldvik, A., T. Gammelsrød, S. Østerhus, E. Fahrbach, G. Rohardt, M. Schröder, K. Nicholls, L. Padman, and R. Woodgate (2004), Ice shelf water overflow and bottom water formation in the southern Weddell Sea, *J. Geophys. Res.*, *109*, C02015, doi:10.1029/2003JC002008.

Gordon, A. L. (1998), Western Weddell Sea thermohaline stratification, in *Ocean, Ice and Atmosphere: Interactions at the Antarctic Continental Margin*, *Antarct. Res. Ser.*, vol. 75, edited by S. Jacobs and R. Weiss, pp. 215–240, AGU, Washington, D. C.

Gordon, A. L., E. Zambianchi, A. Orsi, M. Visbeck, C. F. Giulivi, T. Whitworth III, and G. Spezie (2004), Energetic plumes over the western Ross Sea continental slope, *Geophys. Res. Lett.*, *31*, L21302, doi:10.1029/2004GL020785.

Gordon, A. L., A. H. Orsi, R. Muench, B. A. Huber, E. Zambianchi, and M. Visbeck (2009), Western Ross Sea continental slope gravity currents, *Deep Sea Res., Part II*, *56*, 796–817, doi:10.1016/j.dsr2.2008.10.037.

Holland, D. M., and A. Jenkins (1999), Modeling thermodynamic ice–ocean interactions at the base of an ice shelf, *J. Phys. Oceanogr.*, *29*, 1787–1800, doi:10.1175/1520-0485(1999)029<1787:MTIOIA>2.0.CO;2.

Jackson, L., R. W. Hallberg, and S. Legg (2008), A parameterization of shear-driven turbulence for ocean climate models, *J. Phys. Oceanogr.*, *38*, 1033–1053, doi:10.1175/2007JPO3779.1.

Johnson, G. C. (2008), Quantifying Antarctic Bottom Water and North Atlantic Deep Water volumes, *J. Geophys. Res.*, *113*, C05027, doi:10.1029/2007JC004477.

Legg, S., R. W. Hallberg, and J. B. Girton (2006), Comparison of entrainment in overflows simulated by z-coordinate, isopycnal, and non-hydrostatic models, *Ocean Modell.*, *11*, 69–97, doi:10.1016/j.ocemod.2004.11.006.

Muench, R. D., L. Padman, A. L. Gordon, and A. H. Orsi (2009), A dense water outflow from the Ross Sea, Antarctica: Mixing and the contribution of tides, *J. Mar. Syst.*, *77*, 369–387, doi:10.1016/j.jmarsys.2008.11.003.

Nof, D. (1983), The translation of isolated cold eddies on a sloping bottom, *Deep Sea Res., Part A*, *30*, 171–182, doi:10.1016/0198-0149(83)90067-5.

Noormets, R., J. A. Dowdeswell, R. D. Larter, C. Ó. Cofaigh, and J. Evans (2009), Morphology of the upper continental slope in the Bellingshausen and Amundsen Seas—Implications for sedimentary processes at the shelf edge of West Antarctica, *Mar. Geol.*, *258*, 100–114, doi:10.1016/j.margeo.2008.11.011.

Özgökmen, T. M., and P. F. Fischer (2008), On the role of bottom roughness in overflows, *Ocean Modell.*, *20*, 336–361, doi:10.1016/j.ocemod.2007.10.004.

Özgökmen, T. M., P. F. Fischer, J. Duan, and T. Iliescu (2004), Three-dimensional turbulent bottom density currents from a high-order spectral element model, *J. Phys. Oceanogr.*, *34*, 2006–2026, doi:10.1175/1520-0485(2004)034<2006:TTBDCF>2.0.CO;2.

Padman, L., S. L. Howard, A. H. Orsi, and R. D. Muench (2009), Tides of the northwestern Ross Sea and their impact on dense outflows of high salinity shelf water, *Deep Sea Res., Part II*, *56*, 818–834, doi:10.1016/j.dsr2.2008.10.026.

Rintoul, S. (1998), On the origin and influence of Adèlie Land Bottom Water, in *Ocean, Ice and Atmosphere: Interactions at the Antarctic Continental Margin*, *Antarct. Res. Ser.*, vol. 75, edited by S. Jacobs and R. Weiss, pp. 151–171, AGU, Washington, D. C.

Wåhlin, A. K. (2002), Topographic steering of dense currents with application to submarine canyons, *Deep Sea Res., Part I*, *49*, 305–320, doi:10.1016/S0967-0637(01)00058-9.

Wåhlin, A. K. (2004a), Downward channelling of dense water in topographic corrugations, *Deep Sea Res., Part I*, *51*, 577–590, doi:10.1016/j.dsr.2003.11.002.

Wåhlin, A. K. (2004b), Topographic advection of dense bottom water, *J. Fluid Mech.*, *510*, 95–104, doi:10.1017/S0022112004009590.

Wåhlin, A., and G. Walin (2001), Downward migration of dense bottom currents, *Environ. Fluid Mech.*, *1*, 257–279, doi:10.1023/A:1011520432200.

Wåhlin, A. K., E. Darelius, C. Cenedese, and G. F. Lane-Serff (2008), Laboratory observations of enhanced entrainment in dense overflows in the presence of submarine canyons and ridges, *Deep Sea Res., Part I*, *55*, 737–750, doi:10.1016/j.dsr.2008.02.007.

R. Hallberg, Geophysical Fluid Dynamics Laboratory, NOAA, P.O. Box 308, Princeton, NJ 08542, USA.

R. D. Muench, Earth and Space Research, 10533 Ravenna Ave. NE, Seattle, WA 98125-7745, USA. (rmuench@esr.org)

T. M. Özgökmen, RSMAS, University of Miami, 4600 Rickenbacker Cswy., Miami, FL 3314-1098, USA.

L. Padman, Earth and Space Research, 3350 SW Cascade Ave., Corvallis, OR 97333-1536, USA.

A. K. Wåhlin, Department of Earth Sciences, University of Gothenburg, Box 100, SE-405 30 Göteborg, Sweden.